Momentum and Heat Transfer Phenomena for Power–Law Liquids in Assemblages of Solid Spheres of Moderate to Large Void Fractions

Article *in* Numerical Heat Transfer Applications · December 2009

DOI: 10.1080/10407780903508070

CITATIONS
10

READS
400

4 authors, including:

Nanda Kishore
Indian Institute of Technology Guwahati
169 PUBLICATIONS **2,868** CITATIONS
SEE PROFILE

Raj Chhabra
Indian Institute of Technology Kanpur
402 PUBLICATIONS **12,433** CITATIONS
SEE PROFILE

Vinayak Eswaran
Indian Institute of Technology Hyderabad
186 PUBLICATIONS **6,980** CITATIONS
SEE PROFILE

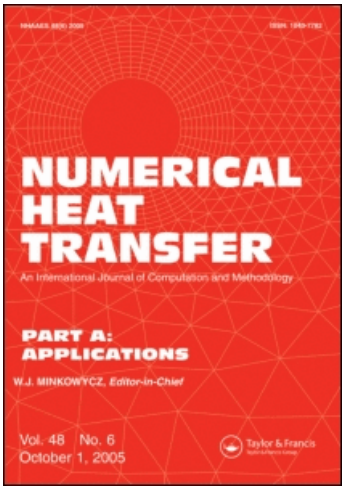

Numerical Heat Transfer, Part A: Applications
Publication details, including instructions for authors and subscription information:
http://www.informaworld.com/smpp/title~content=t713657973

Momentum and Heat Transfer Phenomena for Power-Law Liquids in Assemblages of Solid Spheres of Moderate to Large Void Fractions

N. Kishore [a]; S. D. Dhole [b]; R. P. Chhabra [b]; V. Eswaran [c]
[a] Department of Chemical Engineering, National Institute of Technology, Warangal, India [b] Department of Chemical Engineering, Indian Institute of Technology, Kanpur, India [c] Department of Mechanical Engineering, Indian Institute of Technology, Kanpur, India

Online publication date: 11 January 2010

To cite this Article Kishore, N., Dhole, S. D., Chhabra, R. P. and Eswaran, V.(2009) 'Momentum and Heat Transfer Phenomena for Power-Law Liquids in Assemblages of Solid Spheres of Moderate to Large Void Fractions', Numerical Heat Transfer, Part A: Applications, 56: 12, 970 — 986
To link to this Article: DOI: 10.1080/10407780903508070
URL: http://dx.doi.org/10.1080/10407780903508070

Numerical Heat Transfer, Part A, 56: 970–986, 2009

ISSN: 1040-7782 print/1521-0634 online
DOI: 10.1080/10407780903508070

Taylor & Francis
Taylor & Francis Group

MOMENTUM AND HEAT TRANSFER PHENOMENA FOR POWER–LAW LIQUIDS IN ASSEMBLAGES OF SOLID SPHERES OF MODERATE TO LARGE VOID FRACTIONS

N. Kishore[1], S. D. Dhole[2], R. P. Chhabra[2], and V. Eswaran[3]

[1]*Department of Chemical Engineering, National Institute of Technology, Warangal, India*

[2]*Department of Chemical Engineering, Indian Institute of Technology, Kanpur, India*

[3]*Department of Mechanical Engineering, Indian Institute of Technology, Kanpur, India*

This work extends our previously reported results for the flow of and heat transfer from expanded beds of solid spheres to power–law fluids by using a modified and more accurate numerical solution procedure. Extensive results have been obtained to elucidate the effects of the Reynolds number (Re), the Prandtl number (Pr), the power–law index (n), and the bed voidage (ε) on the flow and heat transfer behavior of assemblages of solid spheres in the range of parameters: $1 \le Re \le 200$, $1 \le Pr \le 1000$, $0.6 \le n \le 1.6$, and $0.7 \le \varepsilon \le 0.999999$. The large values of bed voidage are included here to examine the behavior in the limit of an isolated sphere. As compared to Newtonian fluids, for fixed values of the Reynolds number and the voidage, the total drag coefficient decreases and the average Nusselt number increases for shear thinning fluids ($n < 1$); whereas, for shear thickening fluids ($n > 1$), the opposite behavior is observed. The drag results corresponding to bed voidage, $\varepsilon = 0.99999$, are very close to that of a single sphere; whereas, the heat transfer results approach this limit at $\varepsilon = 0.999$. Based on the present numerical results, simple correlations for drag coefficient and average Nusselt number are proposed which can be used to calculate the pressure drop for the flow of a power–law fluid through a bed of particles, or rate of sedimentation in hindered settling and the rate of heat transfer in assemblages of solid spheres in a new application. Broadly speaking, all else being equal, shear-thinning behavior promotes heat transfer, whereas shear-thickening behavior impedes it.

1. INTRODUCTION

In recent years, considerable research efforts have been expended on elucidating the role of power–law rheology on momentum and heat/mass transfer in particulate systems. In particular, during the last 5–10 years, extensive numerical results have been reported on the steady flow of and heat transfer to Newtonian and power–law fluids through beds of spherical particles over the following ranges of conditions: fractional void volume of the bed, 0.4 to 0.6; power–law index, 0.5 to

Received 19 August 2009; accepted 5 November 2009.

Address correspondence to R. P. Chhabra, Department of Chemical Engineering, Indian Institute of Technology Kanpur, Kanpur-208016, Uttar Pradesh, India. E-mail: chhabra@iitk.ac.in

NOMENCLATURE

C_d	total drag coefficient $\left(=\frac{\boldsymbol{F}_d}{(1/2)\rho \boldsymbol{U}_o^2 \pi \boldsymbol{R}^2} = \boldsymbol{C}_{dp} + \boldsymbol{C}_{df}\right)$, dimensionless
C_{df}	friction drag coefficient $\left(=\frac{2^{n+2}}{\mathrm{Re}}\int_0^\pi \{\tau_{rr}\cos\theta\sin\theta - \tau_{r\theta}\sin^2\theta\}_{r=1} d\theta\right)$, dimensionless
C_{dp}	pressure drag coefficient $\left(=2\int_0^\pi [p\sin 2\theta]_{r=1} d\theta\right)$, dimensionless
C_p	heat capacity, $\mathrm{J/kg \cdot K}$
d	diameter of sphere, m
F_d	total drag force, N
h	convective heat transfer coefficient, $\mathrm{W/m^2K}$
k	thermal conductivity, W/mK
m	power-law consistency index, $\mathrm{Pa \cdot s^n}$
n	power-law behavior index, dimensionless
Nu_θ	local Nusselt number $\left(=\frac{\boldsymbol{hd}}{\boldsymbol{k}} = -2\left[\frac{\partial \boldsymbol{T}}{\partial r}\right]_{r=1}\right)$, dimensionless
$\mathrm{Nu}_{\mathrm{avg}}$	average Nusselt number $\left(=\frac{1}{2}\int_0^\pi \mathrm{Nu}_\theta \sin\theta \boldsymbol{d}\theta\right)$, dimensionless
p	pressure, dimensionless
Pe	Peclet number $(=\mathrm{Re}\times\mathrm{Pr})$, dimensionless
Pr	Prandtl number $\left(=\frac{C_p m}{k}\left(\frac{U_o}{d}\right)^{n-1}\right)$, dimensionless
r	radial distance, dimensionless
R	radius of sphere, m
Re	Reynolds number $\left(=\frac{\rho U_o^{(2-n)} d^n}{m}\right)$, dimensionless
R_∞	cell radius, dimensionless
SMAC	simplified marker and cell
T	fluid temperature, dimensionless
T_o	fluid temperature in the free stream, K
T_s	fluid temperature on the surface of the sphere, K
U_o	free stream velocity of the liquid, m/s
v_r	r – component of velocity, dimensionless
v_θ	θ – component of velocity, dimensionless
v_ϕ	ϕ – component of velocity, dimensionless
ε	fractional void volume, dimensionless
$\in$	rate of strain tensor, $\mathrm{s^{-1}}$
θ	streamwise direction, degree
ϕ	azimuthal direction, degree
$\Pi_\in$	second invariant of the rate of strain tensor, $\mathrm{s^{-2}}$
η	viscosity, $\mathrm{Pa \cdot s}$
ρ	density of liquid, $\mathrm{kg/m^3}$

1.8, Reynolds number, 1 to 500; and Peclet number, 1 to 500 [1–9]. These results have been obtained by numerically solving the continuity, momentum, and energy equations within the framework of the commonly used free surface or the zero vorticity cell models [10, 11] to account for inter-particle interactions. The numerical values of the drag coefficient can, in turn, be related to a suitably defined friction factor to develop an equation akin to the usual Ergun equation for estimating the frictional pressure drop for the flow of power–law fluids through beds of spheres. Suffice it to say here that the resulting predictions of drag coefficient and Nusselt numbers were shown to be in reasonable agreement with the limited experimental results available in the literature; thereby inspiring confidence in the validity of this approach. However, owing to the highly nonlinear nature of the momentum equations (both inertial and viscous terms), it became evident that the use of an uniform grid spacing in the radial direction, as employed in references [2–4, 9] was grossly inadequate with the increasing value of the bed voidage (i.e., increasing radius of the fluid envelope surrounding each particle), especially beyond $\varepsilon > 0.6$ and, hence, these results were limited to the values of bed voidage $\varepsilon \leq 0.6$. On the other hand, bed voidage values up to 0.9 or even larger are encountered in highly expanded fluidized beds [6, 11–14]. Similarly, such dilute systems are also relevant in the hindered settling of particles in power–law fluids to ensure the stability of several pharmaceutical, food, and personal care products under static conditions during their storage

[15], and to ensure trouble free operation of slurry pipelines transporting low concentration suspensions. Finally, there is an additional motivation to extend these results to extremely small values of solid concentration to examine the applicability of the cell model approach to recover the single particle drag coefficient and Nusselt number results by progressively increasing the size of the hypothetical fluid envelope surrounding the particle [16–18]. Thus, these three objectives provide the motivation for this study. In particular, reported herein are the new results on momentum and heat transfer phenomena for the flow of power law fluids through beds of spherical particles over the following ranges of conditions: $0.7 \leq \varepsilon \leq 0.999999$, $0.6 \leq n \leq 1.6$, $1 \leq \mathrm{Re} \leq 200$, and $1 \leq \mathrm{Pe} \leq 20000$. Since the pertinent previous literature has been surveyed elsewhere, it is not repeated here [2–4, 6, 11].

2. PROBLEM STATEMENT AND DESCRIPTION

Consider the steady and incompressible flow of an inelastic power–law fluid through an assemblage of solid spheres of uniform size (radius R or diameter d) maintained at a constant surface temperature, as shown in Figure 1*a*. No temperature gradients exist within the sphere, i.e., the Biot number is small. Within the framework of the free surface cell model, inter – particle hydrodynamic interactions are approximated by postulating that each sphere be surrounded by a hypothetical envelope of fluid of radius R_∞, as shown in Figure 1*b*. The size of the fluid envelope is chosen such that the voidage of each cell is equal to the overall mean voidage of the assemblage. Due to the ϕ – symmetry, the ϕ – component of the velocity vector is zero and no flow variable depends upon the ϕ – coordinate. Under these conditions, the flow and heat transfer characteristics are governed by the equations of continuity, momentum, and energy. In conservative form, these can be written in their dimensionless forms as follows.

Continuity equation

$$\frac{1}{r^2}\frac{\partial}{\partial r}\left[r^2 v_r\right] + \frac{1}{r\sin\theta}\frac{\partial}{\partial\theta}\left[v_\theta \sin\theta\right] = 0 \tag{1}$$

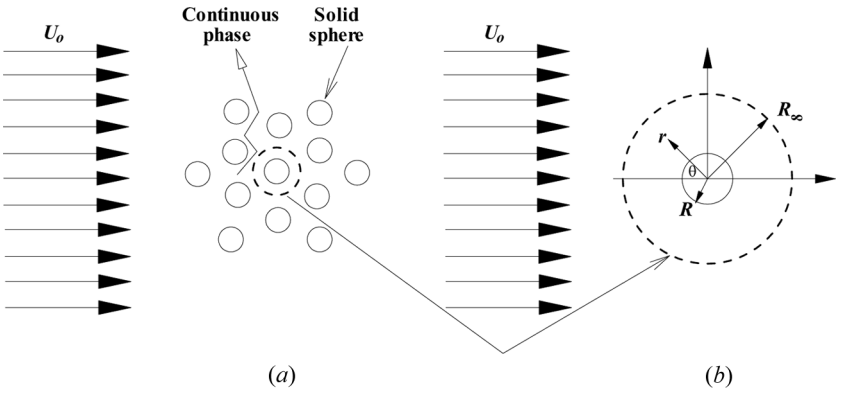

Figure 1. (*a*) Schematic representation of the flow and (*b*) the cell model idealization.

r–component of momentum equation

$$\frac{\partial v_r}{\partial t}+\frac{1}{r^2}\frac{\partial}{\partial r}\left[r^2 v_r^2\right]+\frac{1}{r\sin\theta}\frac{\partial}{\partial\theta}\left[v_r v_\theta \sin\theta\right]-\frac{v_\theta^2}{r}=-\frac{\partial p}{\partial r}+\frac{2^{n+1}}{\mathrm{Re}}\left[\in_{rr}\frac{\partial\eta}{\partial r}+\frac{\in_{r\theta}}{r}\frac{\partial\eta}{\partial\theta}\right]$$
$$+\frac{2^n\eta}{\mathrm{Re}}\left[\frac{1}{r^2}\frac{\partial^2}{\partial r^2}\left(r^2 v_r\right)+\frac{1}{r^2\sin\theta}\frac{\partial}{\partial\theta}\left(\sin\theta\frac{\partial v_r}{\partial\theta}\right)\right] \tag{2a}$$

θ–component of momentum equation

$$\frac{\partial v_\theta}{\partial t}+\frac{1}{r^2}\frac{\partial}{\partial r}\left[r^2 v_r v_\theta\right]+\frac{1}{r\sin\theta}\frac{\partial}{\partial\theta}\left[v_\theta^2\sin\theta\right]+\frac{v_r v_\theta}{r}=-\frac{1}{r}\frac{\partial p}{\partial\theta}+\frac{2^{n+1}}{\mathrm{Re}}\left[\in_{r\theta}\frac{\partial\eta}{\partial r}+\frac{\in_{\theta\theta}}{r}\frac{\partial\eta}{\partial\theta}\right]$$
$$+\frac{2^n\eta}{\mathrm{Re}}\left[\frac{1}{r^2}\frac{\partial}{\partial r}\left(r^2\frac{\partial v_\theta}{\partial r}\right)+\frac{1}{r^2}\frac{\partial}{\partial\theta}\left(\frac{1}{\sin\theta}\frac{\partial}{\partial\theta}\left[v_\theta\sin\theta\right]\right)+\frac{2}{r^2}\frac{\partial v_r}{\partial\theta}\right] \tag{2b}$$

Energy equation

$$\frac{\partial T}{\partial t}+\frac{1}{r^2}\frac{\partial}{\partial r}\left[r^2 v_r T\right]+\frac{1}{r\sin\theta}\frac{\partial}{\partial\theta}\left[v_\theta T\sin\theta\right]=\frac{2}{\mathrm{Pe}}\left\{\frac{1}{r^2}\frac{\partial}{\partial r}\left[r^2\frac{\partial T}{\partial r}\right]+\frac{1}{r^2\sin\theta}\frac{\partial}{\partial\theta}\left[\sin\theta\frac{\partial T}{\partial\theta}\right]\right\} \tag{3}$$

Since the same scaling parameters have been used here to render the above-noted equations dimensionless, as in our previous studies [2–4], these are not repeated here.

The power–law viscosity is given by

$$\eta=\left(\frac{\Pi_\in}{2}\right)^{(n-1)/2} \tag{4}$$

where $\Pi_\in$ is the second invariant of the rate of deformation tensor, which can be expressed in terms of the velocity components and their derivatives [19].

The thermophysical properties (m, n, ρ, k, C_p) of the liquid medium are assumed to be independent of the temperature. Furthermore, viscous dissipation is assumed to be negligible. While these two assumptions lead to the decoupling of the momentum and energy equations, at the same time these also restrict the applicability of these results to the situations, wherein the temperature difference ΔT is small so that these properties of the fluid do not vary appreciably in the flow domain.

The dimensionless radius of the cell, R_∞, is related to the mean voidage of the assemblage as follows.

$$R_\infty=(1-\varepsilon)^{-1/3} \tag{5}$$

Therefore, by simply varying the value of R_∞, one can simulate the beds of various voidages including the limiting case of a single sphere by setting $R_\infty\to\infty$, i.e., $\varepsilon\to 1$. Conversely, one can readily calculate the value of R_∞ for known values of the bed voidage and the size of the sphere. The dimensionless boundary conditions for this flow configuration are written as follows.

At the cell boundary ($r = R_\infty$)

$$v_r = -\cos\theta \tag{6a}$$

$$\tau_{r\theta} = 0 \tag{6b}$$

$$T = 0 \tag{6c}$$

Along the axis of symmetry ($\theta = 0,\ \pi$)

$$v_\theta = 0; \quad \frac{\partial v_r}{\partial \theta} = 0 \tag{7a}$$

$$\frac{\partial T}{\partial \theta} = 0 \tag{7b}$$

On the surface of the sphere ($r = 1$)

$$v_r = 0 \tag{8a}$$

$$v_\theta = 0 \tag{8b}$$

$$T = 1 \tag{8c}$$

However, the role of the far field boundary conditions for the flow over a sphere has been a matter of discussion for many years, especially for the case of multiple particle systems. Detailed comparisons between the values of the drag coefficients obtained by using different boundary conditions either at the cell boundary (in the case of multiple particles) or far away from the particle (in the case of single spheres) have been made by various authors [6]. For instance, Cliffe and Lever [20] have studied the effect of grid size in the stream function – vorticity formulation and the velocity – pressure formulation and found that fairly accurate results can be obtained by using relatively a coarser grid together with the velocity – pressure formulation. Thus, in this study the velocity – pressure formulation in conjunction with relatively finer grids (as will be discussed in the subsequent section) has been used, thereby inspiring confidence and lending support to the accuracy of the results reported herein.

Since the thickness of the momentum and thermal boundary layers on the surface of the sphere progressively decreases with the increasing Reynolds and/or Peclet numbers, a very fine grid is required near the surface of the sphere. An exponential ($y = \ln r$) transformation has been used in the radial direction as used by many others to circumvent this difficulty [21–25]. Equations (1)–(3) subject to the appropriate boundary conditions (Eqs. (6)–(8)) provide the theoretical framework to map the flow domain ($1 \le r \le r_\infty$) in terms of v_r, v_θ, p, and T. Once the fully converged velocity, pressure, and temperature profiles are known, one can readily evaluate the individual and total drag coefficients, the local and average Nusselt numbers as detailed elsewhere [26–32].

3. NUMERICAL METHODOLOGY

3.1. Numerical Details

The governing Eqs. (1)–(3), together with the appropriate boundary conditions, have been solved numerically using a finite-difference method-based SMAC-implicit algorithm implemented on a staggered grid arrangement, which is a simplified version of MAC method due to Harlow and Welch [33]. Since detailed descriptions of the solution procedure for the momentum and energy equations for power–law fluids are presented elsewhere [2–4, 26–32], hence, it is not repeated here. The fully converged steady velocity, pressure, and temperature profiles are used to evaluate the derived quantities such as the individual and total drag coefficients, the local and average Nusselt numbers as functions of the Reynolds number, Peclet number, bed voidage, and power–law index as discussed elsewhere [2–4, 26–32].

3.2. Grid Independence

Needless to emphasize here, the accuracy and reliability of the results are contingent upon a prudent choice of an optimal grid, which inevitably reflects a tradeoff between the level of accuracy required vis-a-vis the computational resources. In this study, we have solved the momentum and energy equations in a segregated manner. Hence, the grid independence tests were carried out only for the momentum equation and, subsequently, the same grid was used for the energy equation without any further testing. This is thought to be satisfactory as the boundary layer shows a stronger dependence on the Reynolds number than that on the Prandtl number. Table 1 shows the effect of the varying grid size in r- and θ- directions for the flow of a Newtonian fluid in assemblages of solid spheres of different voidages. At $\mathrm{Re} = 200$, for $\varepsilon = 0.99$ (i.e., $R_\infty = 4.6416$) and $\varepsilon = 0.999$ (i.e., $R_\infty = 10$), three different grids of sizes 60×60, 60×90, and 90×90 have been used and all three grids produced results which are within $\pm 0.5\%$ of each other. For $\varepsilon = 0.99999$ (i.e., $R_\infty = 46.4158$) at $\mathrm{Re} = 200$, three different grids of sizes 60×120, 60×150, and 90×150 have been used. Grids 60×120 and 60×150 yielded results that are within $\pm 0.2\%$, but the grid 90×150 gave results that are about 0.8% higher than those obtained by 60×120 at an expense of large CPU time. Beyond

Table 1. Grid independence study of a Newtonian fluid flow through assemblages of spheres for different values of bed voidages

Grid	C_{dp}	C_{df}	C_d	C_{dp}	C_{df}	C_d
	$\varepsilon = 0.99$ (i.e., $R_\infty = 4.6416$), $\mathrm{Re} = 200$			$\varepsilon = 0.999$ ($R_\infty = 10$), $\mathrm{Re} = 200$		
60×60	0.4951	0.3854	0.8806	0.4209	0.3523	0.7732
60×90	0.4949	0.3830	0.8779	0.4216	0.3491	0.7707
90×90	0.4958	0.3911	0.8869	0.4213	0.3564	0.7777
	$\varepsilon = 0.99999$ ($R_\infty = 46.4158$), $\mathrm{Re} = 200$			$\varepsilon = 0.999999$ ($R_\infty = 100$), $\mathrm{Re} = 20$		
60×120	0.4108	0.3449	0.7557	0.9906	1.7096	2.7002
60×150	0.4113	0.3435	0.7548	0.9973	1.6999	2.6972
90×150	0.4113	0.3511	0.7624	0.9969	1.7171	2.7140

$\varepsilon = 0.99999$, for large values of Reynolds numbers, the effect of voidage is found to be small; however, at low Reynolds numbers, it does have a significant effect. This is simply due to the slow decay of the velocity field at low Reynolds numbers. Thus, for instance, for $\varepsilon = 0.999999$ (i.e., $R_\infty = 100$), the maximum value of the Reynolds number is restricted to 50. For $\varepsilon = 0.999999$ at $\mathrm{Re} = 20$, three different grids of sizes 60×120, 60×150, and 90×150 have been used and all three produced results within $\pm 0.5\%$ of each other. Therefore, for $\varepsilon = 0.99$ and for $\varepsilon = 0.999$, a grid of size 60×60 whereas, for $\varepsilon = 0.99999$ and for $\varepsilon = 0.999999$, a grid of size 60×120 have been used in this study for all values of pertinent variables.

4. RESULTS AND DISCUSSION

Dimensional considerations of the governing equations and boundary conditions suggest the total and individual drag coefficients to be functions of the Reynolds number, bed voidage, and power–law index; whereas, the Nusselt number shows additional dependence on Prandtl or Peclet number. These relationships are explored in this work. In particular, extensive numerical results have been obtained over the following ranges of parameters: $\mathrm{Re} = 1$, 10, 20, 50, 100, 200; $\mathrm{Pr} = 1$, 10, 50, 100, 500, 1000 (maximum Peclet number is restricted to 20000); $n = 0.6$, 0.8, 1, 1.2, 1.4, 1.6; and $\varepsilon = 0.7$, 0.9, 0.99, 0.999, 0.99999, 0.999999 to explore the functional relationship between these parameters. Therefore, the maximum value of the Prandtl number is determined by the value of the Reynolds number and the above-noted maximum value of the Peclet number.

4.1. Validation

The numerical solver used in this work has been thoroughly benchmarked for various cases involving the flow of Newtonian and power–law fluids over single particles and in clusters of bubbles, drops and solid particles [26–32]. In this work, only additional comparisons are shown in Table 2 for the flow of Newtonian ($n = 1$) and shear-thinning ($n < 1$) fluids through beds of solid spheres of voidage 0.7 and 0.9 at low Reynolds numbers ($\mathrm{Re} = 1$). The present results are seen to be within $\pm 1\%$ to the approximate upper and lower bound results of Mohan and Raghuraman [34]. However, the present results deviate from those of Jaiswal et al. [17] increasingly with the decreasing values of the power–law index. This is thought to be so due to the rather coarse grid used by Jaiswal et al. [17]. Furthermore, the present solver has been validated by comparing the present values of the drag coefficient for the case of $\varepsilon = 0.99999$ with the recent literature values for a single sphere settling in

Table 2. Comparison of present values of drag coefficient at $\mathrm{Re} = 1$

	$\varepsilon = 0.7$			$\varepsilon = 0.9$		
	$n = 1$	$n = 0.8$	$n = 0.6$	$n = 1$	$n = 0.8$	$n = 0.6$
Jaiswal et al. [17]	243.3	140.7	78.16	74.48	56.40	40.32
Mohan and Raghuraman [34]	243.12	149.04	90.96	74.64	58.32	45.36
Present	242.502	148.276	90.147	74.936	58.578	45.571

Table 3. Comparison of present values of C_d for the case of $\varepsilon = 0.99999$ with those of single solid spheres setting in Newtonian and shear-thinning liquids

Re	Present	Song et al. [35]	Dhole et al. [36]	Graham and Jones [38]	Tripathi et al. [37]
			$n = 1$		
10	4.419	4.311	4.28	4.21	4.31
50	1.583	1.577	1.55	1.69	1.55
100	1.089	1.089	1.06	1.11	1.02
			$n = 0.8$		
10	4.278	4.176	4.09	4.21	4.17
50	1.398	1.402	1.37	1.46	1.40
100	0.932	0.938	0.92	0.96	0.92
			$n = 0.6$		
10	3.720	4.015	3.77	4.09	3.76
50	1.174	1.219	1.17	1.26	1.19
100	0.760	0.787	0.76	0.83	0.78

power–law liquids at intermediate Reynolds numbers (Table 3). It is clearly seen that the present results are in excellent agreement with that of Song et al. [35], Dhole et al. [36], and Tripathi et al. [37], though the present results deviate from those of Graham and Jones [38] due to the confinement or wall effects imposed by them. Thus, it is safe to infer that the results for $\varepsilon = 0.99999$ are almost identical to that for a single solid sphere falling in shear-thinning and in Newtonian liquids.

On the other hand, the present heat transfer results are in excellent agreement with the approximate analytical result of Pfeffer [39], numerical results of Mao and Wang [1], and of Shukla et al. [4], as seen in Tables 4–6 and discrepancies are of the order of ±3–4%. It is useful to add here that Shukla et al. [4] also employed an uniform grid spacing in the radial direction whence the accuracy of their results deteriorates rapidly with the increasing value of bed voidage or the radius of the fluid envelope, R_∞. Furthermore, the differences of this magnitude are not at all uncommon in such numerical studies and are frequently ascribed to the differences in the numerical aspects such as, solution procedure, grid, convergence criterion, discretization errors, etc. [40]. Based on these comparisons and our previous experience [2–4, 26–32], the present results are believed to be reliable and accurate within ±3–4%.

4.2. Drag Phenomena

Figure 2 shows the effect of the bed voidage on the total drag coefficient, C_d, as a function of the Reynolds number, Re, for different values of the power–law

Table 4. Comparison of present values of average Nusselt number at $\mathrm{Re} = 1$

	$\varepsilon = 0.7$		$\varepsilon = 0.9$	
Pe	Pfeffer [39]	Present	Pfeffer [39]	Present
500	15.908	16.537	11.788	12.281
1000	20.043	20.630	14.852	15.223

Table 5. Comparison of present values of j_D ($=\mathrm{Nu}/\mathrm{RePr}^{1/3}$) at $\mathrm{Re}=100$

	$\varepsilon=0.7$		$\varepsilon=0.9$	
Pe	Mao and Wang [1]	Present	Mao and Wang [1]	Present
100	0.110	0.106	0.090	0.087
1000	0.100	0.104	0.085	0.084

index (n). Irrespective of the value of the power–law index, as the value of Re and/or of ε increases, the drag coefficient decreases thereby suggesting the lowering of the resistance to flow. As the value of ε increases, the inter-particle separation increases which weakens particle-particle interactions thereby reducing the velocity gradients in the vicinity of spheres and thus lowers the value of the drag coefficient. However, for $\varepsilon > 0.999$, the drag values are little influenced by the value of the bed voidage. This is also seen in Figure 2, where the results for an unconfined single sphere almost coincide with that for $\varepsilon = 0.99999$, at least for Newtonian ($n=1$) and shear-thickening ($n>1$) fluids. However, for shear-thinning fluids ($n<1$) and for small values of the Reynolds number, significant difference is observed. This is probably due to the slow decay of the velocity field at low Reynolds numbers in shear-thinning fluids. For $\varepsilon = 0.9$, as the value of the power–law index increases, the value of C_d increases for all values of the Reynolds number. Conversely, all else being equal, the drag is reduced below its Newtonian value in shear-thinning fluids and it is augmented above its Newtonian value in shear-thickening fluids. Qualitatively, for all values of the power–law index, the value of C_d is large for small values of ε (i.e., small R_∞) which gradually decreases as the value of bed voidage increases and approaches the value of a single solid sphere. However, for $\varepsilon = 0.99$ and $\varepsilon = 0.999$,

Table 6. Comparison of the present values of average Nusselt number at intermediate Reynolds and Peclet numbers

		$\varepsilon=0.6$		$\varepsilon=0.8$	
Re	Pe	Shukla et al. [4]	Present	Shukla et al. [4]	Present
			$n=0.6$		
1	20	8.091	8.031	5.834	5.728
	1000	26.736	25.306	20.391	19.126
100	200	17.237	16.594	14.375	13.495
	1000	31.751	29.553	25.949	23.603
			$n=1$		
1	20	8.027	7.982	5.699	5.632
	1000	24.842	23.904	18.558	17.845
100	200	15.303	14.907	12.468	12.006
	1000	26.499	25.315	21.250	20.141
			$n=1.6$		
1	20	–	7.947	–	5.560
	1000	–	22.951	–	16.967
100	200	14.130	13.871	10.996	10.772
	1000	23.764	23.033	18.188	17.646

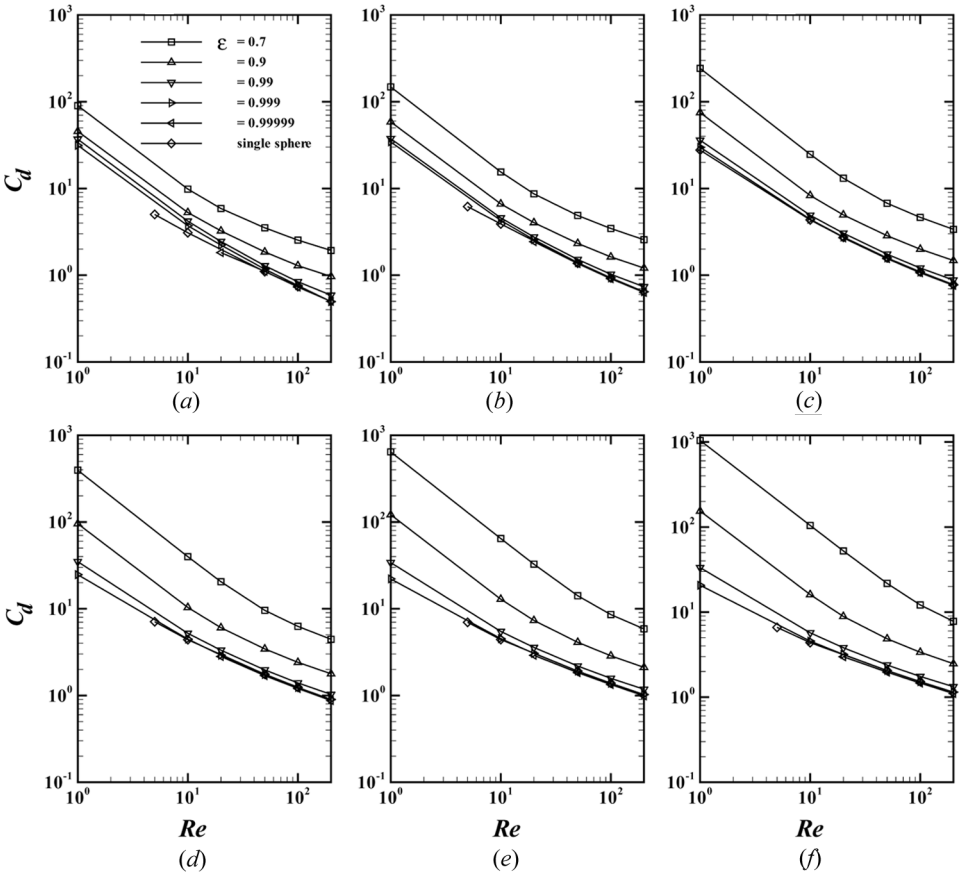

Figure 2. Effect of void fraction of bed on drag coefficient as a function of Reynolds number for different values of power–law index. (*a*) $n = 0.6$, (*b*) $n = 0.8$, (*c*) $n = 1.0$, (*d*). $n = 1.2$, (*e*) $n = 1.4$, and (*f*) $n = 1.6$.

the effect of the power–law index on the value of C_d is rather weak for small values of Reynolds number; however, the effect of the power–law index increases as the value of the Reynolds number gradually increases. Similar trends can be seen for C_{dp} and C_{df}. In summary, for all values of bed voidage and Reynolds number, the value of C_d increases as the value of n increases. These trends are also consistent with that reported by Dhole et al. [36] and more recently by Song et al. [35].

Finally, the present numerical results have been correlated using the following equation.

$$C_d = \left[0.9 + 0.01\mathrm{Re}^{0.98}(1-\varepsilon)^{0.11}\right]\left(\frac{2^{n+3}}{\mathrm{Re}}\right) \left[\frac{\left(\frac{2n+1}{2n}\right) + 2[1-\varepsilon]^{(4n+1)/(2n+1)}}{1-(3/2)[1-\varepsilon]^{n/(4n-1)} + (3/2)[1-\varepsilon]^{(4n+1)/(2n+1)} - [1-\varepsilon]^2}\right] \tag{9}$$

The above equation reproduces the present numerical results (174 data points) with an average error of ±16.58%, which rises to maximum of ±33.69% for large

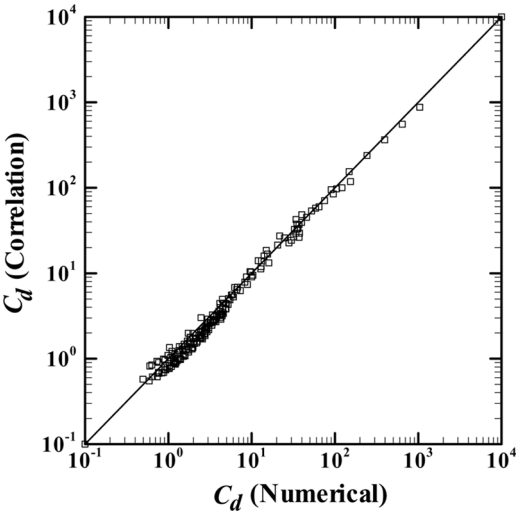

Figure 3. Parity plot between numerical and correlated values of total drag coefficient.

values of the void fraction when $n \leq 1$ and $\mathrm{Re} \geq 100$. For a given system, usually the values of *m, n,* ε, and the size of the solid particles are known, and the only unknown is the drag coefficient (or sedimentation velocity). Thus, Eq. (9) can be used to estimate this value. Figure 3 shows the parity plot between the numerical and predicted values (from Eq. (9)) of drag coefficient and no discernable trends are observed with Reynolds number or power–law index or void fraction or any combinations thereof.

4.3. Heat Transfer Phenomena

Figure 4 shows the effect of voidage, ε, on the variation of the local Nusselt number on the surface of the sphere along the θ – direction, i.e., on Nu_θ for different values of power–law index at $\mathrm{Re} = 100$ and $\mathrm{Pr} = 100$. Irrespective of the value of the power–law index, since no flow separation occurs for $\varepsilon = 0.7$ and 0.9 at this value of the Reynolds number, the local value of the Nusselt number, Nu_θ, decreases continually from the front stagnation point all the way up to the rear stagnation point. For all values of n and for $\varepsilon \geq 0.99$, the value of Nu_θ decreases up to the separation point and then increases up to the rear stagnation point. However, for all values of ε and for $n \leq 1$, as one traverses from the front stagnation point of the sphere, the local value of Nu_θ increases up to some point on the surface of the sphere (depending on the values of ε and n, $\theta \approx 20$–25°) before it begins to decrease up to the separation point. As expected, the effect of bed voidage, ε, on the Nusselt number diminishes for $\varepsilon \geq 0.999$, as also noted earlier for drag phenomena. For all values of ε, the effect of n is seen to be significant only up to the point of separation or in the first half of the sphere surface, i.e., up to $\theta \approx 90$–110°.

Figure 5 shows representative results elucidating the effect of Prandtl number on the local Nusselt number in a shear-thinning fluid, $n = 0.6$ (Figures 5*a*–5*c*) and in a shear-thickening fluid, $n = 1.6$ (Figures 5*d*–5*f*) for different values of ε at $\mathrm{Re} = 200$. The different levels of distortion in isotherms in the rear of the sphere are evident in

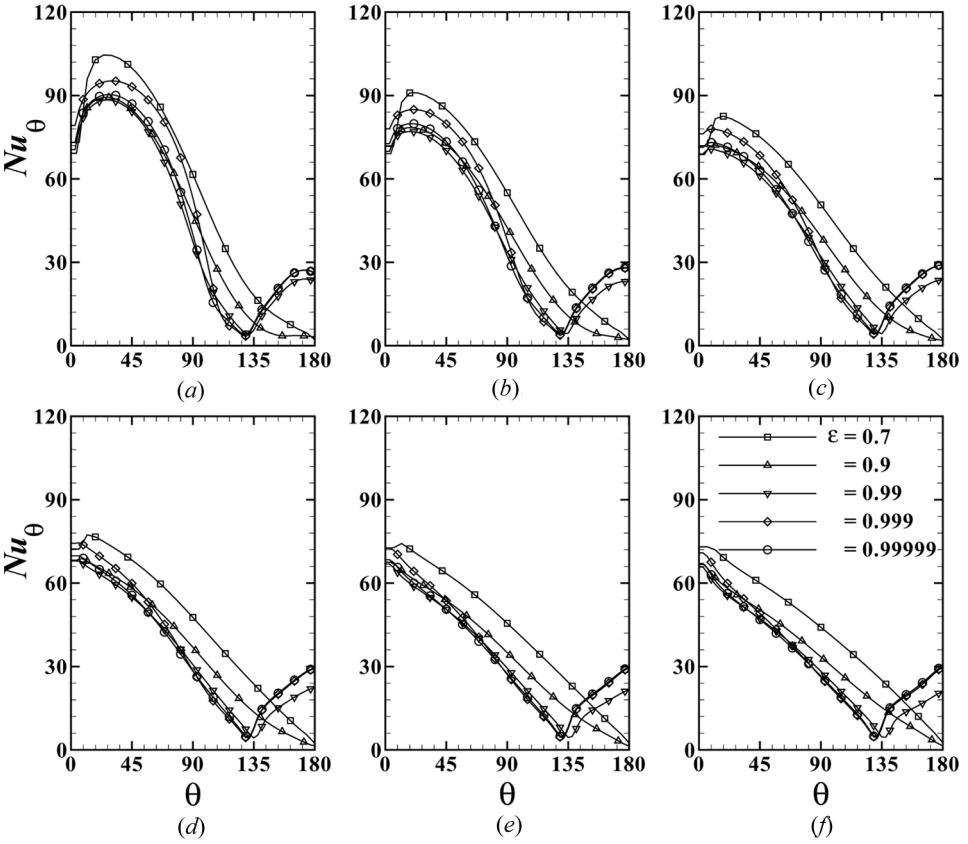

Figure 4. Effect of void fraction of bed on local Nusselt number at $\mathrm{Re} = 100$ and $\mathrm{Pr} = 100$ for different values of power–law index. (*a*) $n = 0.6$, (*b*) $n = 0.8$, (*c*) $n = 1$, (*d*) $n = 1.2$, (*e*) $n = 1.4$, and (*f*) $n = 1.6$.

this figure in the form of variation in Nu_θ for different values of Pr. For large values of Pe, the rise of Nu_θ in the rear is more significant than that for moderate values of the Peclet numbers. Also, as seen earlier (Figure 4), for shear-thinning fluids there is a significant rise in the local value of Nu_θ, up to $\theta \approx 20$–60° depending on the values of ε and Pr; whereas, for shear-thickening fluid it decreases from the front stagnation point. This is due to the two competing effects namely, the decreasing values of the temperature gradients and increasing/decreasing viscosity depending upon the value of the power–law index.

Figures 6*a*–6*c* show typical results demonstrating the effect of voidage, ε, on the average Nusselt number; $\mathrm{Nu}_{\mathrm{avg}}$ as a function of Pe for different values of n for $\mathrm{Re} = 10$. For all values of n and ε, as the value of the Peclet number increases, the average Nusselt number $\mathrm{Nu}_{\mathrm{avg}}$ increases. For all values of n, as the value of ε increases, it decreases because of the lowering of the temperature gradients due to weak inter-particle interactions. Similarly, Figures 6*d*–6*f* show the effect of power–law index n on the average Nusselt number $\mathrm{Nu}_{\mathrm{avg}}$ for a range of values of ε. For all values of ε, the average Nusselt number, $\mathrm{Nu}_{\mathrm{avg}}$ in a shear-thinning fluid is larger than that in a Newtonian fluid; whereas, it is lower in a shear-thickening fluid.

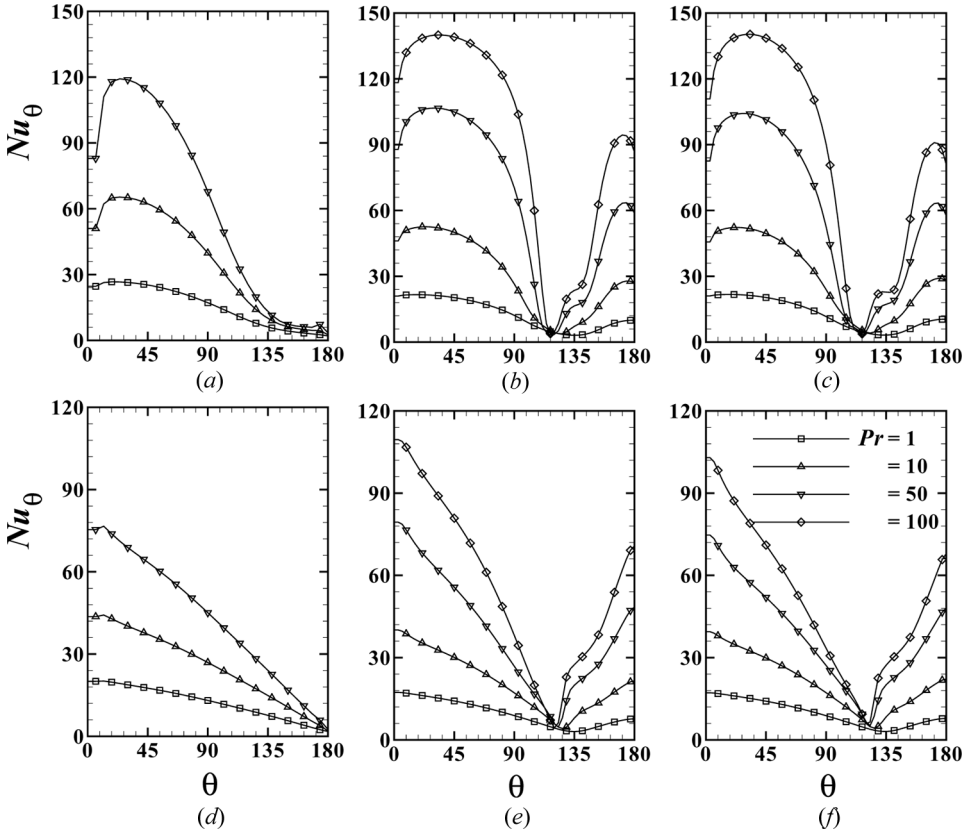

Figure 5. Effect of Prandtl number on local Nusselt number in a shear-thinning fluid, $n = 0.6$ (*a*)–(*c*) and in a shear-thickening fluid, $n = 1.6$ (*d*)–(*f*) at $\mathrm{Re} = 200$ for different values of void fractions of bed. (*a*) $\varepsilon = 0.7$, (*b*) $\varepsilon = 0.999$, (*c*) $\varepsilon = 0.99999$, (*d*) $\varepsilon = 0.7$, (*e*) $\varepsilon = 0.999$, and (*f*) $\varepsilon = 0.99999$.

However, the effect of ε and of *n* seems to be significant only at large values of Peclet number/Prandtl number, i.e., when the thermal boundary layer is very thin. Thus, as expected, shear-thinning fluid behavior promotes heat transfer whereas shear-thickening behavior impedes it.

Finally, based on the present numerical results, the following simple correlation has been proposed for the average Nusselt number;

$$\mathrm{Nu}_{\mathrm{avg}} = 0.922 + \mathrm{Re}^{1/(n+2)}\mathrm{Pr}^{1/3}\varepsilon^{-5/3} + 0.1\mathrm{Re}^{2/3}\mathrm{Pr}^{1/3} \tag{10}$$

Equation (10) reproduces the present results with an average error of ±5.94% which rises to a maximum of ±40% for small Peclet numbers (<10) and small values of void fractions. However, there are theoretical results or correlations already available for $\mathrm{Pe} = 1$ which can be used for $\mathrm{Pe} \leq 1$ [6]. The above equation reduces to that of Dhole et al. [41] for the case of heat transfer from a heated single solid sphere to power–law fluids, which further reduces to the result of Feng and Michaelides [21] for Newtonian fluids. Figure 7 shows the parity plot between the numerical and

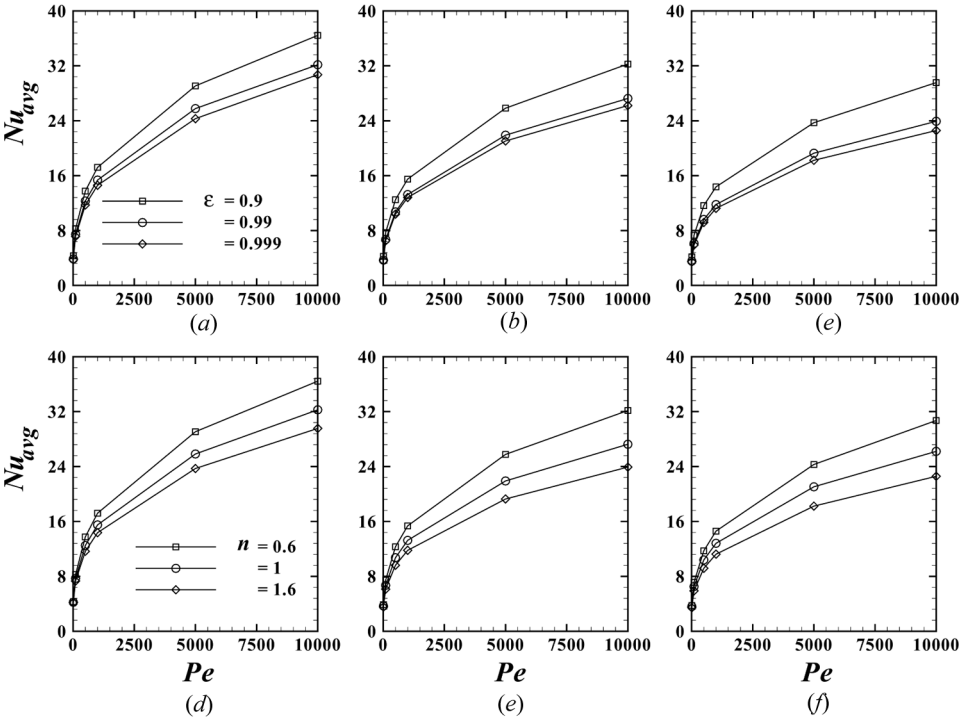

Figure 6. Effect of power–law index and void fraction of bed on average Nusselt number as a function of Peclet number at Re = 10. (*a*) $n = 0.6$, (*b*) $n = 1$, (*c*) $n = 1.6$, (*d*) $\varepsilon = 0.9$, (*e*) $\varepsilon = 0.99$, and (*f*) $\varepsilon = 0.999$.

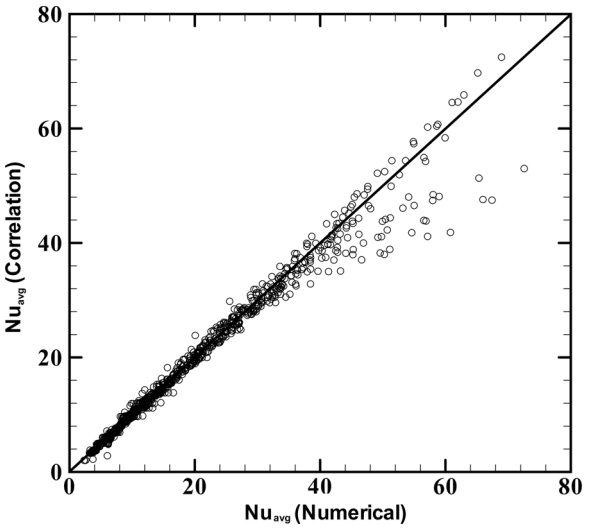

Figure 7. Parity plot between numerical and correlated values of the average Nusselt number.

calculated values of the average Nusselt number. Once again, there are no discernable trends present except for the case of large values of Peclet numbers.

5. CONCLUSION

As compared to Newtonian fluids, for fixed values of the Reynolds number and the voidage, the total drag coefficient decreases and the average Nusselt number increases for shear thinning fluids ($n < 1$); whereas, the opposite behavior is observed in shear thickening fluids ($n > 1$). As the value of the power–law index increases, the value of C_{dp}/C_{df} was seen to decrease for all combinations of the Reynolds number and the bed voidage. For all values of the bed voidage, the effect of the power–law index on the local Nusselt number is more significant up to the point of flow separation. For fixed values of the Peclet number, as the value of the bed voidage and/or of the power–law index increases, the average Nusselt number decreases. The drag results for $\varepsilon = 0.99999$ are very close to that of a single sphere; whereas, the heat transfer results approach this limiting behavior even at $\varepsilon = 0.999$. Finally, the present numerical results are used to develop correlations for drag coefficient and average Nusselt number, which can be used to calculate the rate of sedimentation in hindered settling or pressure drop across a bed of particles, and the rate of interphase heat transfer in assemblages of solid spheres.

REFERENCES

1. Z. S. Mao and Y. Wang, Numerical Simulation of Mass Transfer of a Spherical Particle Assemblage with the Cell Model, *Powder Tech.*, vol. 134, pp. 145–155, 2003.
2. S. D. Dhole, R. P. Chhabra, and V. Eswaran, Power–Law Fluid Flow through Beds of Spheres at Intermediate Reynolds Numbers: Pressure Drop in Fixed and Distended Beds, *Chem. Eng. Res. Des.*, vol. 82, pp. 642–652, 2004.
3. R. Shukla and R. P. Chhabra, Effect of Non-Newtonian Characteristics on Convective Liquid-Solid Heat Transfer in Packed and Fluidized Beds of Spherical Particles, *Can. J. Chem. Eng.*, vol. 82, pp. 1071–1075, 2004.
4. R. Shukla, S. D. Dhole, R. P. Chhabra, and V. Eswaran, Convective Heat Transfer for Power–Law Fluids in Packed and Fluidized Beds of Spheres, *Chem. Eng. Sci.*, vol. 59, pp. 645–659, 2004.
5. F. A. Coutelieris, M. E. Kainourgiakis, and A. K. Stubos, Low to Moderate Peclet Mass Transport in Assemblages of Spherical Particles for a Realistic Adsorption-Reaction-Desorption Mechanism, *Powder Tech.*, vol. 159, pp. 173–179, 2005.
6. R. P. Chhabra, *Bubbles, Drops, and Particles in Non-Newtonian Fluids*, 2nd ed., CRC Press, Boca Raton, FL, USA, 2006.
7. Z. S. Mao, C. Yang, and Y. Wang, Effectiveness Factor of a Catalytic Sphere in Particle Assemblage Approached with a Cell Model, *Chem. Eng. Sci.*, vol. 62, pp. 6475–6485, 2007.
8. G. Juncu, Unsteady Conjugate Forced Convection Heat/Mass Transfer in Ensembles of Spherical Particles with Cell Models, *Int. J. Heat Mass Transfer*, vol. 52, pp. 1817–1826, 2009.
9. A. K. Jaiswal, T. Sundararajan, and R. P. Chhabra, Simulation of Non-Newtonian Fluid Flow through Fixed and Fluidized Beds of Spherical Particles, *Numer. Heat Transfer A*, vol. 21, pp. 275–297, 1992.

10. J. Happel, Viscous Flow in Multiparticle Systems: Slow Motion of Fluids Relative to Beds of Spherical Particles, *AIChE J.*, vol. 4, pp. 197–201, 1958.
11. R. P. Chhabra, J. Comiti, and I. Machac, Flow of Non-Newtonian Fluids in Fixed and Fluidized Beds, *Chem. Eng. Sci.*, vol. 56, pp. 1–27, 2001.
12. D. Ciceron, J. Comiti, R. P. Chhabra, and M. Renaud, Non-Newtonian Fluidization of Spherical Particles, *Chem. Eng. Sci.*, vol. 57, pp. 3225–3234, 2002.
13. B. Siska and I. Machac, Fluidization with Viscoelastic Polymer Solutions in the Transition Flow Region, *Chem. Eng. Sci.*, vol. 61, pp. 8089–8094, 2006.
14. L. Broniarz-Press, P. Agacinski, and J. Rozanski, Shear-Thinning Fluids Flow in Fixed and Fluidised Beds, *Int. J. Multiphase Flow*, vol. 33, pp. 675–689, 2007.
15. B. Siska, I. Machac, P. Dolecek, and J. Cakl, Batch Sedimentation of Spherical Particles in Non-Newtonian Liquids, *Proc. 8th Int. Conf. on Transport and Sedimentation of Solid Particles*, Paper # F2, January 24–26, Prague, 1995.
16. A. K. Jaiswal, T. Sundararajan, and R. P. Chhabra, Flow of Power–Law Liquids through Particle Assemblages at Intermediate Reynolds Numbers, *Can. J. Chem. Eng.*, vol. 69, pp. 1235–1241, 1991.
17. A. K. Jaiswal, T. Sundararajan, and R. P. Chhabra, Hydrodynamics of Creeping Flow of Power–Law Fluid Through Particle Assemblages, *Int. J. Eng. Sci.*, vol. 31, pp. 293–306, 1993.
18. A. K. Jaiswal, T. Sundararajan, and R. P. Chhabra, Pressure Drop for the Flow of Dilatant Fluids through a Fixed Bed of Spherical Particles, *Can. J. Chem. Eng.*, vol. 72, pp. 352–353, 1994.
19. R. B. Bird, W. E. Stewart, and E. N. Lightfoot, *Transport Phenomena*, 2nd ed., John Wiley, New York, 2002.
20. K. A. Cliffe and D. A. Lever, A Comparison of Finite Element Methods for Solving Flow Past a Sphere, *J. Comp. Phys.*, vol. 62, pp. 321–330, 1986.
21. Z. G. Feng and E. E. Michaelides, Heat and Mass Transfer Coefficients of Viscous Spheres, *Int. J. Heat Mass Transfer*, vol. 44, pp. 4445–4454, 2001.
22. Z. G. Feng and E. E. Michaelides, Drag Coefficients of Viscous Spheres at Intermediate and High Reynolds Numbers, *Trans. ASME, J. Fluids Eng.*, vol. 123, pp. 841–849, 2001.
23. A. Saboni, S. Alexandrova, A. M. Spacic, and C. Gourdon, Effect of the Viscosity Ratio on the Mass Transfer from a Fluid Sphere at Low to Very High Peclet Pumbers, *Chem. Eng. Sci.*, vol. 62, pp. 4742–4750, 2007.
24. G. Juncu, A Numerical Study of Steady Viscous Flow Past a Fluid Sphere, *Int. J. Heat Fluid Flow*, vol. 20, pp. 414–421, 1999.
25. G. Juncu, Unsteady Heat and/or Mass Transfer from a Fluid Sphere in Creeping Flow, *Int. J. Heat Mass Transfer*, vol. 44, pp. 2239–2246, 2001.
26. N. Kishore, R. P. Chhabra, and V. Eswaran, Sedimentation in Emulsions of Mono-Size Droplets at Moderate Reynolds Numbers, *Chem. Eng. Res. Des.*, vol. 84, pp. 1180–1193, 2006.
27. N. Kishore, R. P. Chhabra, and V. Eswaran, Mass Transfer from Ensembles of Newtonian Fluid Spheres at Moderate Reynolds and Peclet Numbers, *Chem. Eng. Res. Des.*, vol. 85, pp. 1203–1214, 2007.
28. N. Kishore, R. P. Chhabra, and V. Eswaran, Drag on a Single Fluid Sphere Translating in Power–Law Liquids at Moderate Reynolds Numbers, *Chem. Eng. Sci.*, vol. 62, pp. 2422–2434, 2007.
29. N. Kishore, R. P. Chhabra, and V. Eswaran, Mass Transfer from a Single Fluid Sphere to Power–Law Liquids at Moderate Reynolds Numbers, *Chem. Eng. Sci.*, vol. 62, pp. 6040–6053, 2007.

30. N. Kishore, R. P. Chhabra, and V. Eswaran, Drag on Ensembles of Fluid Spheres Translating in Power–Law Liquids at Moderate Reynolds Numbers, *Chem. Eng. J.*, vol. 139, pp. 224–235, 2008.
31. N. Kishore, R. P. Chhabra, and V. Eswaran, Mass Transfer from Ensembles of Fluid Spheres to a Power–Law Liquid at Moderate Reynolds and Peclet Numbers, *Chem. Eng. Sci.*, vol. 63, pp. 2484–2499, 2008.
32. N. Kishore, R. P. Chhabra, and V. Eswaran, Bubble Swarms in Power–Law Liquids at Moderate Reynolds Numbers: Drag and Mass Transfer, *Chem. Eng. Res. Des.*, vol. 86, pp. 39–53, 2008.
33. F. H. Harlow and J. E. Welch, Numerical Calculation of Time-Dependent Viscous Incompressible Flow of Fluid with Free Surfaces, *Phys. Fluids*, vol. 8, pp. 2182–2188, 1965.
34. V. Mohan and J. Raghuraman, A Theoretical Study of Pressure Drop for Non-Newtonian Creeping Flow Past an Assemblage of Spheres, *AIChE J.*, vol. 22, pp. 259–264, 1976.
35. D. Song, R. K. Gupta, and R. P. Chhabra, Wall Effects on a Sphere Falling in Quiescent Power–Law Fluids in Cylindrical Tubes, *Ind. Eng. Chem. Res.*, vol. 48, pp. 5845–5856, 2009.
36. S. D. Dhole, R. P. Chhabra, and V. Eswaran, Flow of Power–Law Fluids Past a Sphere at Intermediate Reynolds Numbers, *Ind. Eng. Chem. Res.*, vol. 45, pp. 4773–4781, 2006.
37. A. Tripathi, R. P. Chhabra, and T. Sundararajan, Power–Law Fluid Flow over Spheroidal Particles, *Ind. Eng. Chem. Res.*, vol. 33, pp. 403–410, 1994.
38. D. I. Graham and T. E. R. Jones, Settling and Transport of Spherical Particles in Power–Law Fluids at Finite Reynolds Number, *J. Non-Newt. Fluid Mech.*, vol. 54, pp. 465–488, 1994.
39. R. Pfeffer, Heat and Mass Transport in Multi-Particle Systems, *Ind. Eng. Chem. Fund.*, vol. 3, pp. 380–383, 1964.
40. P. J. Roache, Perspective: A Method for Uniform Reporting of Grid Refinement Studies, *Trans. ASME, J. Fluids Eng.*, vol. 116, pp. 405–413, 1994.
41. S. D. Dhole, R. P. Chhabra, and V. Eswaran, Forced Convection Heat Transfer from a Sphere to Non-Newtonian Power–Law Fluids, *AIChE J.*, vol. 52, pp. 3658–3667, 2006.